97S-49

In Vivo Thresholds for Mechanical Injury to the Blood-Brain Barrier

David I. Shreiber, Allison C. Bain, and David F. Meaney

Department of Bioengineering, University of Pennsylvania

ABSTRACT

A finite element model of cerebral contusion in the rat was developed and compared to experimental injury maps demonstrating blood-brain barrier (BBB) breakdown. The model was exercised at the nine unique loading conditions used experimentally. Logistic regressions of four variables, maximum principal logarithmic strain (LEP), maximum principal stress (SP), strain energy density (SEN), and von Mises stress (MIS) demonstrated highly significant confidence in the prediction of the 50th percentile values (chi-squared, $p<0.00001$). However, only values for LEP were invariant across loading conditions. These results suggest that the BBB is most sensitive to LEP, and that breakdown occurs above a strain of 0.188 +/- 0.0324.

INTRODUCTION

Finite element analysis (FEA) has become a common tool used by research engineers to study the biomechanics of traumatic brain injury (TBI) (see [1, 2] for review). From early simulations to present ones, FEA has been used to identify both the skull's and/or brain's reactions to various mechanical input conditions, as well as possible tolerance criteria to deleterious variables such as shear strain and pressure [3-5]. Until recently, FEA of TBI concentrated mainly on modeling the human brain. Initially, these models were built to understand the changes in intracranial pressure (ICP) seen experimentally in human cadaver impact studies [3, 6]. Next, models were used to examine the effects of translational and rotational loading conditions [4, 7, 8]. In the past few years, work has begun in simulating real-life situations where complicated loading conditions are taken from crash simulations [9].

With these increasingly complex and accurate finite element models of the human brain, it is now critical to understand the relationship between the stress and strain within the brain and the resulting in vivo neural and/or vascular injury. To develop estimates of in vivo thresholds, engineers have often simulated experimental animal models of TBI. Unlike other surrogates, animal models offer a functional biological system that can respond to a mechanical insult by showing grades of injury to the neural and vascular tissues. With the advent of sophisticated markers for injury at the cellular and molecular level, the analysis of the animal models can form an important and unique step in defining the thresholds for injury to the brain due to impact or impulsive loading conditions.

To date, the analyses of animal models of brain injury have yielded approximate relationships between mechanical parameters and the presence of both vascular and neural damage. Ueno et al. reinvestigated the experimental work of Lighthall by modeling midline cortical impact in the ferret brain, and observed a relationship between the areas of cerebrovascular injury and both von Mises stress and shear strain [8, 10]. Several research groups have focused on a form of neural injury - diffuse axonal injury - and have been successful in drawing relationships between shear stress/strain, cumulative strain, and oriented strain to the presence of axonal injury [9, 11-13].

In this investigation, we develop estimates of the in vivo threshold for mechanical injury to the blood-brain barrier (BBB) using an integrated series of animal experiments and finite element simulations. Currently, the mechanical threshold for BBB breakdown is not well developed even though it is the underlying mechanism for the most frequent form of closed head injury - cerebral contusions [14]. Moreover, the breakdown of the BBB is directly responsible for a portion of the primary neurological deficits appearing after injury, and can be exacerbated by several secondary injury phenomena such as excitotoxicity, edema, and ischemia [14, 15]. By developing in vivo mechanical thresholds for the mildest form of contusion - the opening of the blood-brain barrier - one can eventually identify the circumstances that cause cerebral contusions and

develop better prevention technology for this common form of brain injury.

MATERIALS AND METHODS

EXPERIMENTAL MODEL OF BBB DAMAGE - Dynamic cortical deformation (DCD) is a unique experimental model because it induces a purely focal lesion by exposing the cortex to a dynamic vacuum pulse of clinically relevant (<100 ms) duration. The injury is initiated by triggering the actuation of a solenoid, which is connected to a vacuum source. When the solenoid valve opens, a vacuum pressure pulse is applied to the brain through a specially designed aluminum couple via a Leur-Lock fitting. The dynamic vacuum pressure signal is measured by a pressure transducer (Entran, Fairfield, NJ), filtered and amplified, and sampled by a data acquisition system in an IBM-compatible computer.

In Vivo Cortical Displacement - The in vivo nature of the injury prohibits visualization of the intracranial deformation. However, a laser displacement transducer (Omron, Schaumburg, IL) permits measurement of the displacement of the exposed cortex. The transducer emits a low intensity infrared laser beam which is incident on the cortical surface. The transducer measures displacement according to the position of the reflected beam on the transducer's collector. A calibration procedure was performed prior to each experiment by incrementally moving the laser transducer a prescribed distance with a micromanipulator and recording the resulting voltage at each increment to determine a linear relationship between the output voltage and distance to the cortical surface. These calibrations uniformly had linear regression correlation coefficients (R^2) > 0.97. The dynamic displacement of the cortex was sampled by the data acquisition system. After an analysis of the frequency spectrum of a baseline signal from a rat brain revealed no dominant noise component, a nine-pole digital averaging filter was selected to filter the displacement traces. A schematic of the DCD device is shown in Figure 1.

Surgery and Injury - Adult, male, Sprague-Dawley rats (350-400 g) were anesthetized and placed in a stereotaxic head holder. A 5-mm craniectomy was performed over the left parietal cortex. Under a dissecting microscope, the dura was removed in the region of the craniectomy, thus providing no mechanical resistance to the vacuum pulse. A Leur-Lock fitting was attached over the craniectomy with a cyanoacrylate adhesive and secured with dental cement. The fitting made an air-tight seal with the mechanical couple.

After the dental cement had cured (~20 minutes), animals were given an i.v. dose of 2% Evans Blue dye in saline (2 ml/kg). The dye was permitted to circulate for five minutes to allow all free dye to bind to serum albumin [16]. After five minutes, DCD was performed at the pre-defined loading conditions (Table 1). Ten minutes post-injury, animals were euthanized with a lethal dose of sodium pentobarbital, exsanguinated with 0.9% heparinized saline, and perfused with 10% neutral buffered formalin followed by 10% sucrose in buffered saline. The brains were removed and stored in 30% sucrose until processing. All procedures were approved by the University of Pennsylvania's Institutional Animal Care and Use Committee (IACUC - Protocols 608-0, 608-1, 2887-0).

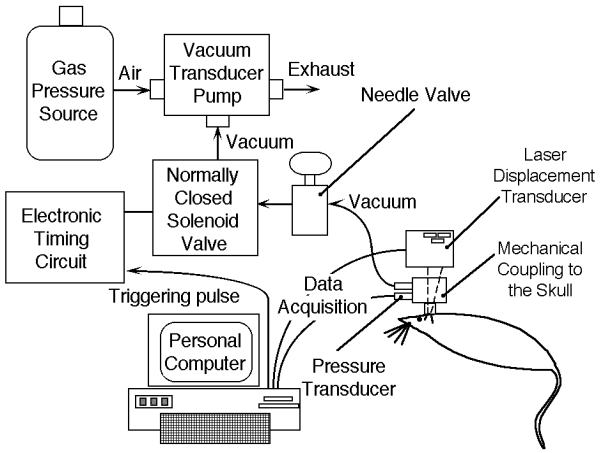

Figure 1: Schematic of DCD device. The device allows independent control of the magnitude, onset rate, and duration of the vacuum pulse. The applied pressure and cortical displacement are recorded by the data acquisition system.

To investigate the effects of changing the loading conditions applied to the cortex during DCD - namely the magnitude and rise time/duration of the vacuum pulse - on BBB breakdown, a 3x3 experimental test matrix was designed (Table 1). Individual groups of animals (n=7) were injured with a vacuum pulse of either 2, 3, or 4 psi (1 psi = 6,895 Pa) magnitude and 25, 50, or 100 msec duration (approximately 12.5, 25, and 50 msec rise time, respectively) (Figure 2). An additional group of animals (n=7) served as sham controls for the surgical procedures.

Table 1: Test matrix for the experimental DCD study

	Magnitude				
Duration	Sham	2 psi	3 psi	4 psi	$n_{duration}$
Sham	7				7
25 msec		7	7	7	21
50 msec		7	7	7	21
100 msec		7	7	7	21
$n_{magnitude}$	7	21	21	21	n_{total} = 70

Measurement of Blood-Brain Barrier (BBB) Breakdown - Each brain was cut coronally around the injury site into a ~2cm block. Frozen coronal sections

(300 microns thick) were cut on a freezing microtome such that consecutive slices were 500 microns apart. Slices were mounted on glass slides and coverslipped.

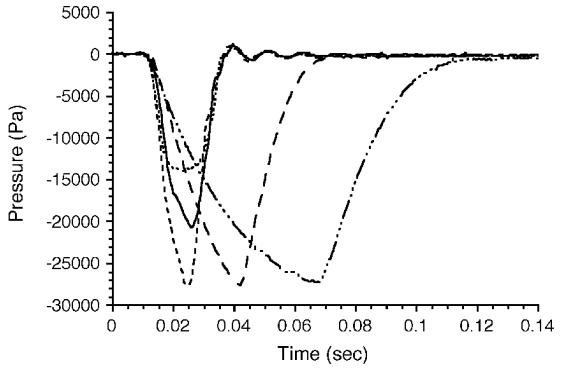

Figure 2: Sample experimental pressure traces demonstrating the different magnitudes and durations used in the study. Experimental DCD was performed at three magnitudes of vacuum pressure over three durations, for a total of nine independent loading conditions.

For the experimental model, we assumed that, at the very short survival time used (10 minutes), the damage to the BBB was purely mechanically mediated. Although the BBB is sensitive to a number of changes in the intracranial environment, including temperature, blood pressure, and surrounding chemicals [17-21], these secondary insults take time - up to days - to develop. Recent studies [20, 22, 23] suggest that, although some molecules which exacerbate BBB damage are released within five minutes after injury, the effects of such molecules are not immediately noticeable. Hence, by selecting a very brief survival duration, we hoped to minimize secondary damage to the BBB and isolate mechanically mediated injury.

To visualize the extent of BBB breakdown, individual slices were photographed with an intensified CCD camera under epifluorescence microscopy (dual FITC/Texas Red barrier filter block, 480 nm excitation, 575 nm emission) to take advantage of the autofluorescent ability of Evans Blue. The resulting signal was strong enough to be seen with a low power (2x) objective. However, even at that low magnification, the field of view only encompassed a fraction of the original slice. Composite images were built by sequencing through the section with a motorized stage and acquiring partial pictures (Metamorph) until the entire section was enveloped.

To quantify the extent of BBB damage, the volume of Evans Blue/albumin extravasation was calculated for each brain. First, for each slice in an individual brain, the area of extravasated dye was calculated by thresholding the image based on a grayscale pixel value taken from control, uninjured tissue from the same brain, and measuring the number of pixels above the threshold value. Individual slice pixel area measurements were summed, converted to area, and multiplied by the linear distance between slices (500 microns) to arrive at the volume of extravasation for the brain.

FINITE ELEMENT MODEL OF BBB DAMAGE - To analyze the mechanics of the experimental model, we developed a finite element model using a commercially available pre-processor (MSC/PATRAN, MSC, Inc.), and analysis code (ABAQUS/EXPLICIT, HKS, Inc.).

Mesh generation - All mesh generation was performed with MSC/PATRAN. The FEM is composed of two homogeneous structures - the brain and the skull (Figure 3). Although there is a distinct gray/white matter structure in the rat brain, the white matter in rodents is truly limited and does not project into the cortex like in humans and other highly developed mammals. For this reason, we felt it was appropriate to model the brain as a single, homogenous structure.

The geometry for the brain was created by digitizing the border of consecutive coronal sections (0.5 mm apart) from a histological atlas of the rat brain [24]. Each section was divided into six simple 4-edge surfaces, which were in turn connected to form 6-faced solids. The solids were meshed with the “Isomesh” feature in MSC/PATRAN. The brain consisted of 36,664 8-node hexahedron "brick" reduced-integration elements. A bilateral region surrounding the craniectomy site was refined to improve the model’s performance in the region of interest and aid in post-processing analysis. Incongruent surfaces were matched using the tied contact surface algorithm available in ABAQUS/EXPLICIT.

The skull was modeled by enlarging the exterior surface of the brain by 5% and connecting surfaces at the sagittal midline. The skull was considered to be a rigid surface. Over the left parietal cortex, a hole was removed from the skull. A hollow, tapered cylindrical surface, modeling the Leur-Lock cap used to apply the vacuum pulse, was built above the hole. The surfaces were meshed with rigid quadrilateral (n=2,404) and triangular (n=16) elements.

Material Properties - The brain was considered to be homogeneous and isotropic. Studies of the material response of brain tissue have demonstrated that brain tissue exhibits non-linear, viscoelastic behavior. We expected large tissue deformations in the simulations; therefore, we used a modified hyperelastic material law over other linear viscoelastic material models [25]. Whereas other non-linear descriptions of brain tissue have been proposed using quasi-linear theory and an instantaneous elastic function [26], the description of a material with a strain energy density function greatly facilitates its use with finite element analysis packages. We selected a value for the

instantaneous shear modulus (3.3 psi =20,684 Pa) that fell within the range of shear moduli for published human brain data [13, 27-31]. No published data exists concerning material properties of the rat brain.

The instantaneous shear modulus was divided into two Mooney-Rivlin hyperelastic constants, C_{01} and C_{10}, based on the ratio proposed by Mendis [25]. Using previous studies of the time-dependent behavior of brain tissue as a guide and adjusting for model performance in comparison to experimental data, we arrived at the following final brain material description [25, 26, 28]:

$$C_{10}(t) = 0.9C_{01}(t) = 5481\left(1 - 0.528e^{\frac{-t}{0.008}} - 0.302e^{\frac{-t}{0.150}}\right) \quad [1]$$

The brain was considered to be purely elastic in dilatation. To expedite the simulations, Poisson's ratio was set at 0.495. A comparison of results using this Poisson's ratio to a simulation using a Poisson's ratio of 0.49999 (effective bulk modulus of 300,000 psi = 2.1 GPa) , revealed less than 3% change in the results.

Loading Conditions - To model the loading conditions, individual experimental vacuum pressure traces were converted into pressure-time data pairs. The pressure was applied to the exposed face of brain elements directly beneath the craniectomy. These elements did not form a perfect circle; thus, any element that could be seen from the top through the craniectomy was considered to be exposed to the vacuum pulse.

Boundary Conditions - Contact was modeled between the skull/cap and the brain; the coefficient of friction was 0.2. The skull/cap was fixed in space.

Model Solution - The finite element simulation was performed using ABAQUS/EXPLICIT on an SGI Origin 2000 with 4 parallel CPU's. The finite element analysis was performed nine times, once at each of the unique loading conditions applied experimentally. An energy balance inspection was performed for each analysis to ensure proper convergence.

Model Validation - The finite element model was validated by comparing the peak displacement of nodes on the model surface exposed to the vacuum pulse to the mean peak cortical displacement measured experimentally for each of the loading conditions. The peak model displacement was determined by averaging the peak displacement for nodes within a 1mm diameter circle at the center of the craniectomy, to approximate the 1mm spot diameter of the laser beam. The criteria for validation was influenced by the variability of the experimental data, and was set at within one standard deviation of the mean experimental peak displacement.

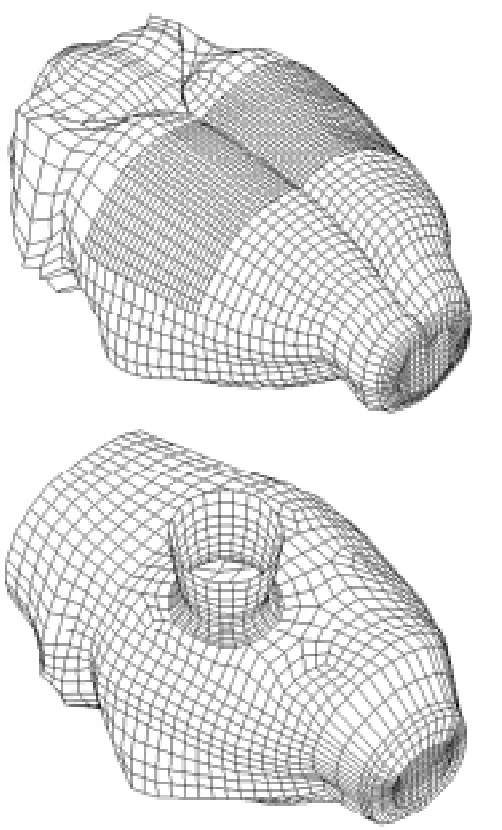

Figure 3: Finite element meshes for the brain (top) and skull. The brain consists of 8-node hexahedron reduced-integration solid elements. Incongruent elements were matched with the tied surface algorithm in ABAQUS/EXPLICIT. The skull and cap consist of rigid 4-node quadrilateral and 3-node triangular elements that were fixed in space.

Data Analysis - Frequently with finite element models, peak values for particular elements or locations are reported and compared to clinical and/or experimental data. This method yields little statistical power, and does not utilize the full extent of information from an animal model. In this study, we compared the finite element mesh to the composite images of BBB breakdown on an element-by-element basis using logistic regressions. The specific form of the logistic regression model used is:

$$\pi(x) = \frac{e^{\alpha+\beta x}}{1+e^{\alpha+\beta x}} \quad [2]$$

This model is more often recognized after the logit transformation:

$$g(x) = ln\left[\frac{\pi(x)}{1-\pi(x)}\right] \quad [3]$$

$$= \alpha + \beta x$$

Logistic regression analysis is a useful statistical technique in determining relationships from binary or discrete data. It is most frequently applied to biological models, but has also been previously used in the injury biomechanics community to identify tolerances and specific measures that best predict risk of injury [32-35]. In this study, we have used logistic regressions to distinguish causal factors for injury to the BBB from measurements taken on populations of "injured" and "uninjured" elements based on our experimental and computational models. Each element can be thought of as an individual subjected to a specific magnitude of stress and/or strain. By dividing the experimental and computational results into elements and comparing the experimental elements to their computational counterpart, we greatly improve the statistical utility of our finite element model for each particular simulation. Moreover, comparing experimental and computational results on an elemental basis with logistic regressions enables mathematical inclusion of spatial results.

This distinguishes the methodology presented herein from other methods of mathematically reducing computational data, such as the Cumulative Strain Damage Measure (CSDM) [7]. The CSDM identifies tolerance criteria for DAI by calculating the cumulative number of elements that experience at least a particular strain magnitude during a simulation. However, whereas this method is useful in quantitatively measuring the "volume" of injury and qualitatively identifying nucleation sites for deleterious strain, in its current state it cannot mathematically relate the effectiveness of the model in predicting the location of high strains. Nevertheless, the CSDM is a novel and interesting technique that we plan to employ as a partial check against our lesion volume data after we have completed the analysis for the remaining 54 cases.

One brain from each of the nine groups was randomly selected for analysis. Three coronal levels from each of these brains were chosen to compare the FEM solution to the experimental data - the rostral border, middle, and caudal border of the craniectomy. At each of these levels, the deformed mesh was superposed over the image from the appropriate coronal level captured under epifluorescence microscopy. The image was filtered such that pixels with a grayscale value greater than that for control, uninjured tissue taken from the same brain were changed to black, and all others changed to gray. Tissue tears were also marked as black. Ventricles and other empty spaces were marked white. Any grid element that overlapped a "black" region was marked as injured; all other elements that overlapped a gray region were marked uninjured (Figure 4). From these elements, sets of random injured and uninjured elements were created (n_{set}=40-150 elements).

To identify mechanical thresholds for BBB breakdown, four variables were evaluated for each simulation using logistic regression techniques - maximum principal logarithmic strain (LEP), maximum principal stress (SP), strain energy density (SEN), and von Mises Stress (MIS). LEP is the principal strain measure provided by the analysis code, and is frequently used in finite strain problems. LEP and SP were included because they are traditionally viewed as mechanical mediators of failure. SEN was included as a potential new variable that combines strain and strain rate effects. MIS was chosen as a measure of the distortional stress, and has been used as a threshold variable by other laboratories [8, 13]. After each simulation, the maximum values of these four variables were recorded for each element in the injured and uninjured sets. Logistic regression plots for each

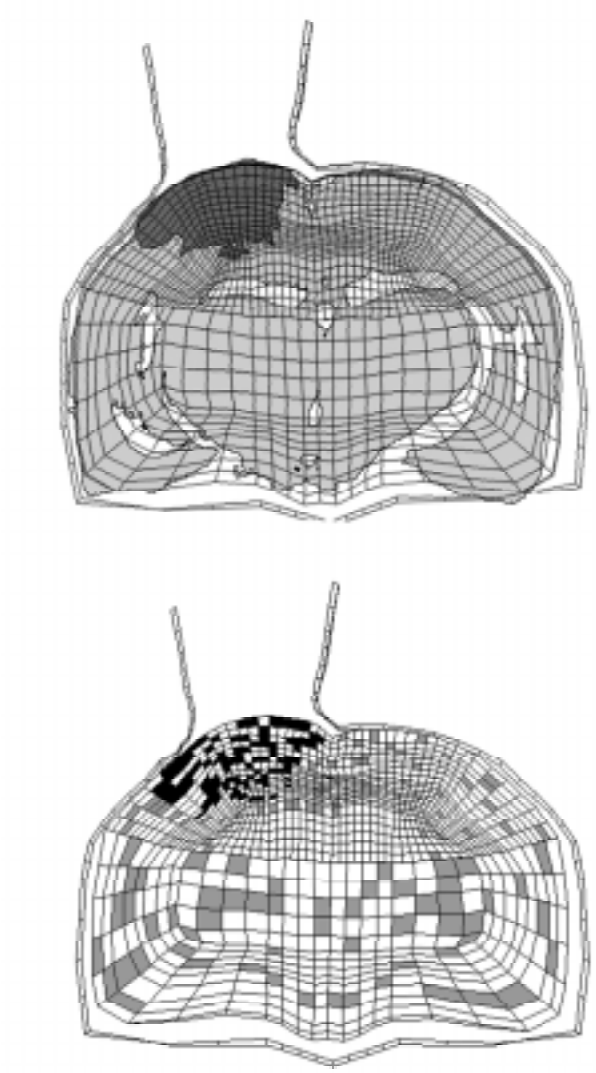

Figure 4: Representative experimental coronal slice after thresholding (top) and element selection map (bottom). For the experimental slice, pixels with grayscale values above a threshold value based on control tissue are black, and all other tissue is gray. In the element map, black elements represent ones chosen for the "injured" set, and gray elements represent ones chosen for the "uninjured" set for this particular slice.

variable were produced, and the 50th percentile value, 95% confidence intervals, and chi-squared significance term were identified (SYSTAT LOGIT Plug-in Module, SPSS Inc, Chicago, IL). From the nine simulation-experiment comparisons, nine thresholds for each variable were produced. The logistic regression fit was considered significant for chi-squared values with $p<0.01$. The threshold data was then analyzed with one-way ANOVA's, with significance set at $p<0.05$.

RESULTS

EXPERIMENTAL MODEL - Figure 5 displays four composite slices taken from the same brain. DCD produced focal damage to the BBB immediately inferior to the craniectomy. Evans Blue/albumin extravasation was evident as "bright" regions under epifluorescence microscopy. Additionally, tissue tears were frequently observed at the ipsilateral gray/white matter junction.

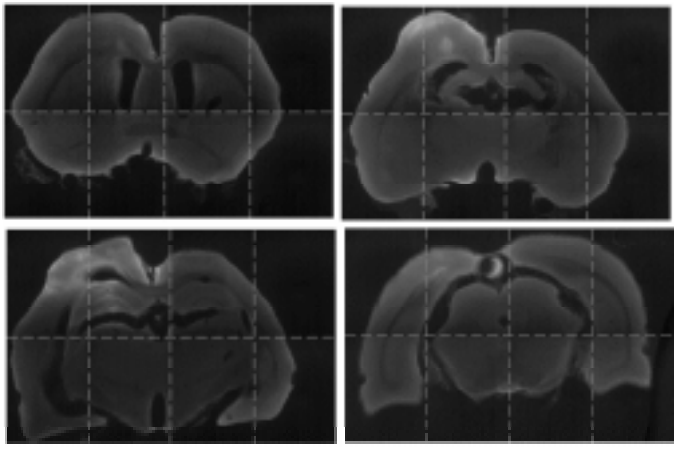

Figure 5: Composite images of coronal slices of the same brain under epifluorescence microscopy taken from the experimental DCD study (4 psi, 100 msec). Images were created by sequencing through the slice with a motorized stage and building a composite of the individual images. Bright regions depict areas of Evans Blue/albumin extravsation.

Lesion Volume - A two-way ANOVA of the lesion volume data demonstrated that the two independent variables, magnitude and duration, were significant effects ($p<0.001$ and $p<0.008$, respectively). Furthermore, the interaction of the two variables was also significant ($p<0.05$). Scheffe's post-hoc tests for significance revealed that increasing the duration from 25 msec to 50 msec caused a significant increase in BBB breakdown ($p<0.04$), whereas increasing from 50 msec to 100 msec did not. Figure 6 graphically depicts the results of the lesion volume calculations for the experimental test matrix.

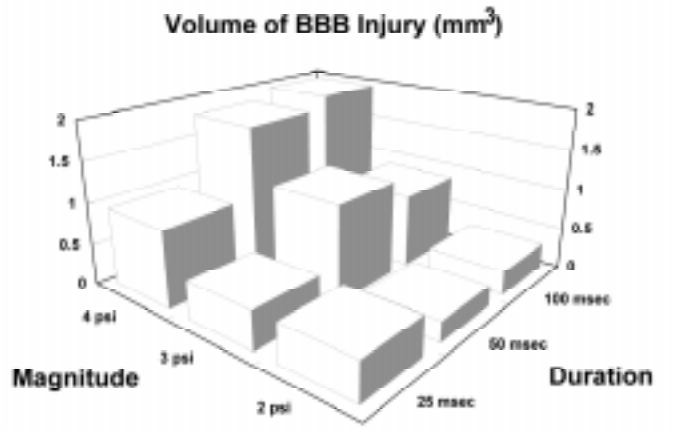

Figure 6: Three dimensional plot of extravasation volume versus duration and magnitude. Both magnitude and duration, as well as their interaction, were found to be significant effects on volume (two-way ANOVA, $p<0.001$, $p<0.008$, $p<0.05$, respectively). Post-hoc examination revealed that the effect of duration was localized to changes from 25 to 50 msec (Scheffe's post-hoc test, $p<0.04$).

Cortical Displacement - Figure 7 displays example pressure and displacement traces from one of the experiments (3 psi, 100 msec). In general, the displacement of the cortex lagged slightly behind the applied vacuum pressure. The cortex did not return to its initial position, but rather demonstrated a degree of long-term or permanent deformation. Peak cortical displacement, measured from these traces, was found to be highly variable. Vacuum pressure magnitude was found to be a significant effect on cortical displacement ($p=0.001$). Duration was not a statistically significant factor for peak displacement.

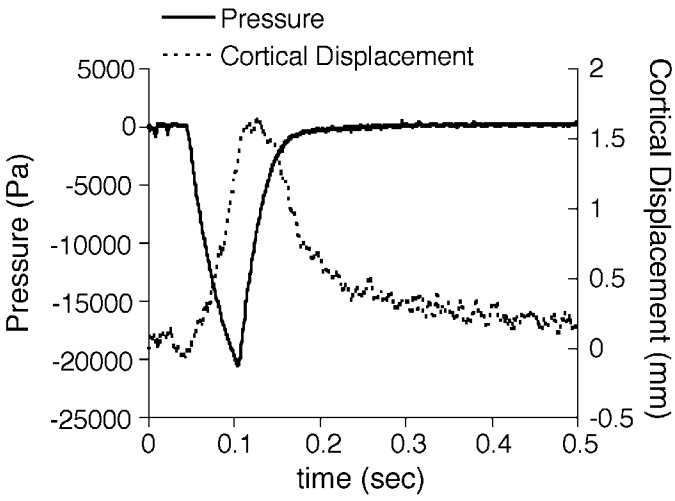

Figure 7: Example experimental pressure and displacement traces from one of the cases (3psi, 100 msec). Displacement lagged slightly behind vacuum pressure, and displayed permanent or long-term deformation.

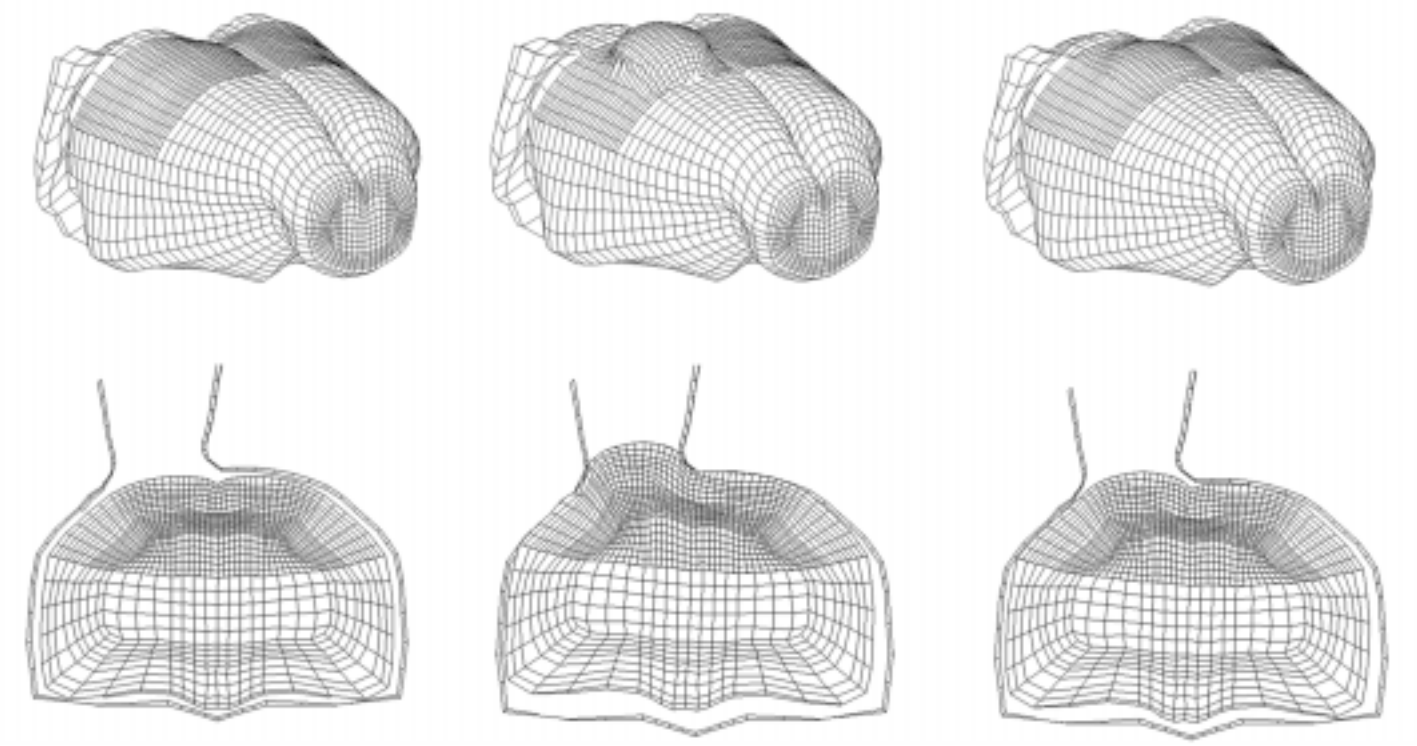

Figure 8: Typical undeformed (left), peak (middle), and final (right) deformation profiles following simulation of DCD for the entire brain and for a coronal slice from the middle of the craniectomy. Similar to the experimental evidence, the deformation was localized to the region immediately inferior to the craniectomy. Contact between the brain and skull/cap occurred. Some shift of midline elements to the ipsilateral side was evident. The model demonstrated a degree of deformation after unloading that resembled experimental cases.

FINITE ELEMENT ANALYSES - Figure 8 demonstrates a typical deformation profile for the entire brain and for a coronal plane taken at the middle of the craniectomy site. The finite element simulations of DCD produced a deformation profile that was similar to the experimental cases. In all cases, contact between the skull/cap and the brain occurred. The final profile of the model demonstrated some permanent deformation due to viscous losses. Peak deformation was localized to the region immediately inferior to the craniectomy (Figure 9). No significant deformation was observed remote from the injury site.

MODEL VALIDATION - Figure 10 displays the experimental cortical displacement data along with the average nodal displacement data from the computational model. The average nodal displacement was within 10% of the mean value for all but two cases, and was within one standard deviation of the mean for simulations of all loading conditions.

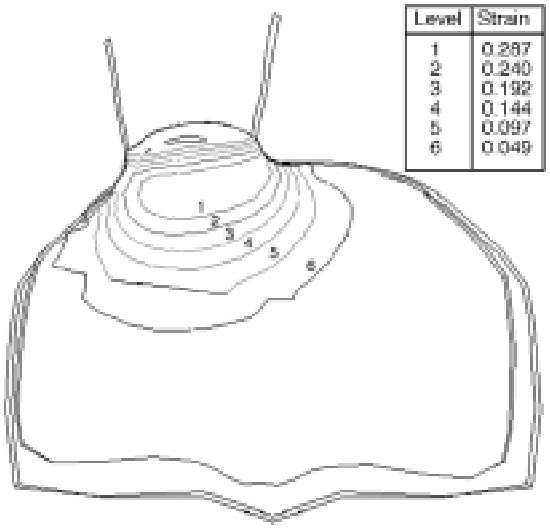

Figure 9: Contour plot of a typical LEP profile at the midline of the craniectomy (25 msec, 4 psi). The strain field was localized to the injury site. SP, SEN, and MIS demonstrated similar profiles.

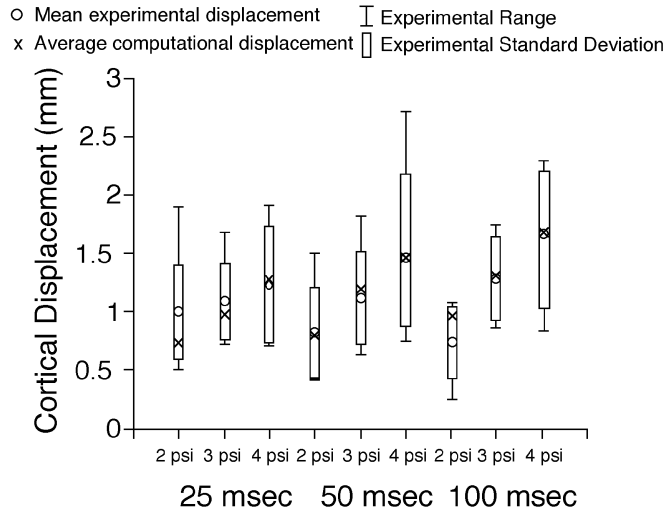

Figure 10: Experimental and computational displacement data for the cortex inferior to the craniectomy. The average nodal displacement from the finite element model was within 10% of the mean peak displacement from the experimental model for all but two loading conditions, and fell within one standard deviation of the mean for all loading conditions.

STATISTICAL ANALYSES - A logistic regression plot from one of the simulation cases (LEP, 3 psi, 50 msec), along with histograms representing the frequency distribution of injured and uninjured elements with respect to LEP, are shown in Figure 11. All of the logistic regressions demonstrated significance at a high level (chi-squared, p<0.00001). Figure 12 shows all of the logistic regressions for the four variables. In general, the slopes of the regressions were the same within and across injury measures. LEP had the tightest grouping of regression curves. Appendix A lists the values for the constants α and β and chi-squared values for the regressions.

The 50th percentile values and the 95% confidence intervals for the individual regressions are shown in Table 2. These values are displayed graphically in Figure 13. From these plots and one-way ANOVA's using duration as the effect, trends governing the threshold values for SP, SEN, and MIS were revealed. For the 3 and 4 psi cases, the threshold values consistently decreased from the 25 msec to the 50 msec cases. This trend was not apparent for LEP. Although the results were not significant, the trend was substantiated by the p-values for the three variables (SP - p=0.146, SEN - p=0.062, MIS - p=0.068). The trend was not evident for the fourth variable, LEP (p=0.645). No trends were observed after one-way ANOVA's using vacuum magnitude as the main effect (minimum p=0.376).

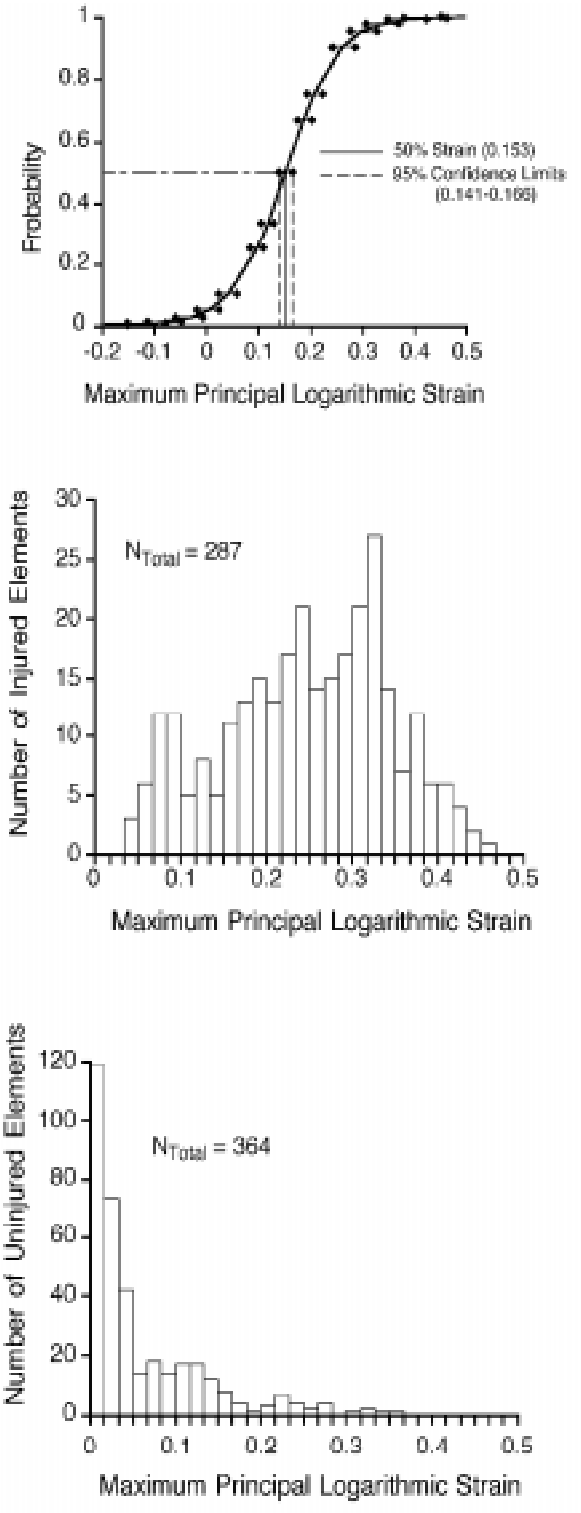

Figure 11: A representative logistic regression (LEP, 3 psi, 50 msec) demonstrating the 50th percentile probability value and 95% confidence limits. Shown beneath the regression are histograms depicting the frequency distribution of the injured and uninjured elements according to LEP. The tight confidence intervals were characteristic of all of the logistic regressions.

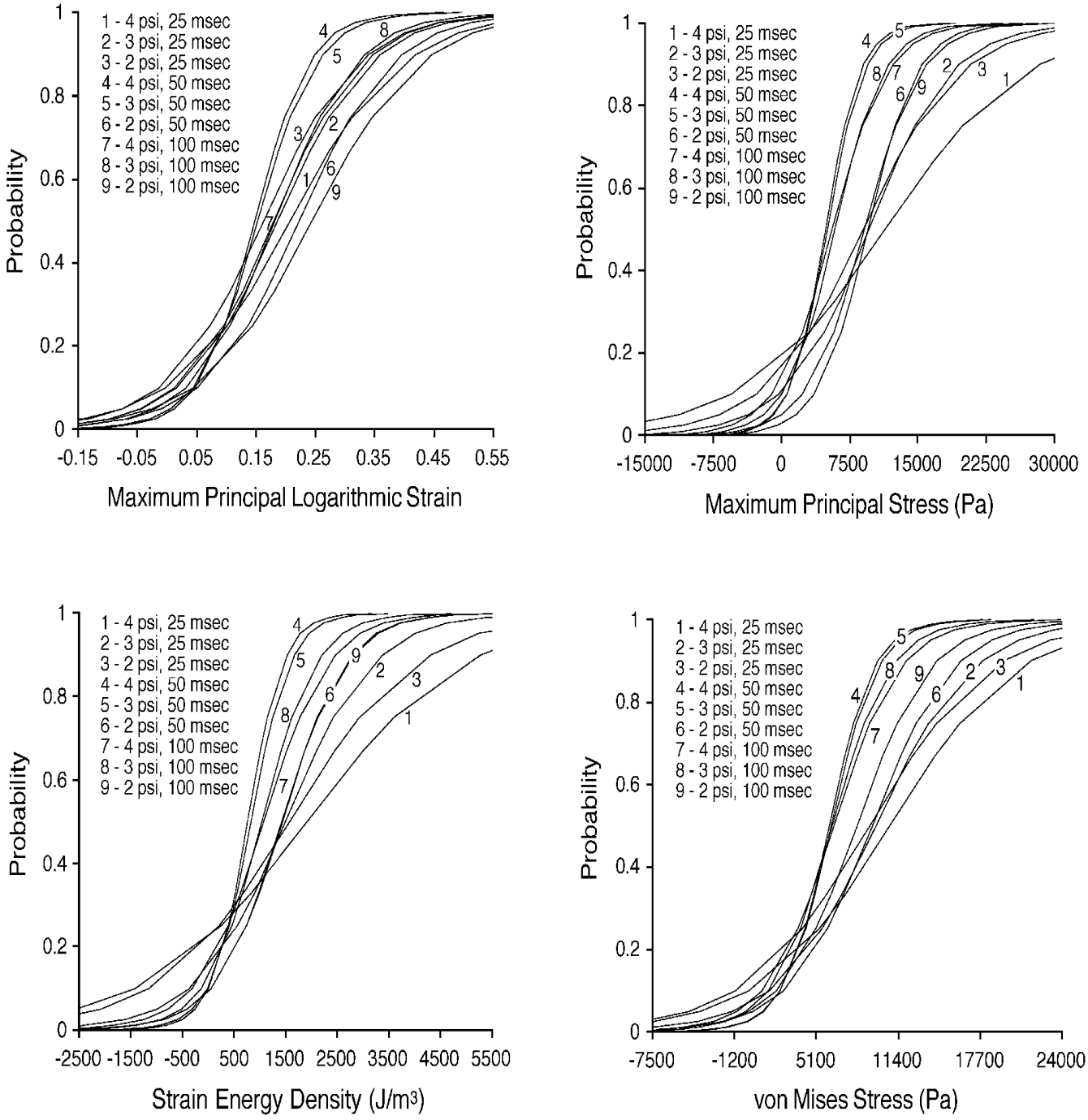

Figure 12: Logistic regression plots for each of the four measures. The regressions demonstrated similar slopes within and across variables. The grouping of curves was tightest for LEP

For a variable to be considered a useful predictor of injury, the 50th percentile - or threshold - value should be consistent regardless of the loading conditions. This was not the case with SP, SEN, or MIS. The 50th percentile value for these variables decreased with increasing duration. The lack of statistical significance for these trends is easily explained by the limited number of degrees of freedom in this particular investigation. The reduction of analyses to one case per unique set of experimental loading conditions effectively eliminated the ability of the ANOVA to detect statistical significance. In the immediate future, we will be completing this analysis for the remainder of the experiments. We believe that the trends reported herein will repeat themselves in the final study, and that the increased number of degrees of freedom will lead to an improved statistical model.

Table 2: 50th percentile "threshold" values and 95% confidence limit for the nine loading conditions and each variable.

		25 msec	50 msec	100 msec
LEP	**4 psi**	0.208 (0.187-0.231)	0.148 (0.138-0.159)	0.180 (0.164-0.198)
	3 psi	0.187 (0.169-0.208)	0.153 (0.141-0.166)	0.182 (0.168-0.198)
	2 psi	0.163 (0.141-0.193)	0.223 (0.200-0.255)	0.245 (0.221-0.276)
		25 msec	**50 msec**	**100 msec**
SP (Pa)	**4 psi**	11430.6 (9819.5-13341.9)	4813.2 (4399.8-5280.2)	5598.4 (4949.1-6342.8)
	3 psi	9649.5 (8533.3-11004.1)	5032.6 (4546.2-5590.4)	5891.9 (5300.8-6569.7)
	2 psi	8988.2 (7478.2-11412.3)	9543.5 (8747.3-10487.1)	9150.2 (8292.3-10180.2)
		25 msec	**50 msec**	**100 msec**
SEN (J/m^3)	**4 psi**	1924.6 (1613.3-2302.5)	767.3 (687.5-861.2)	1079.8 (940.7-1242.2)
	3 psi	1502.2 (1300.0-1755.0)	828.0 (734.2-936.1)	1038.2 (922.9-1171.0)
	2 psi	1579.56 (1156.8-2598.3)	1425.1 (12251.0-1713.4)	1437.5 (12260.0-1673.1)
		25 msec	**50 msec**	**100 msec**
MIS (Pa)	**4 psi**	10761.2 (9693.1-11946.5)	6098.0 (5710.0-6522.4)	6460.0 (5904.2-7060.5)
	3 psi	9670.9 (8790.8-10695.1)	6233.4 (5796.2-6702.7)	6322.1 (5837.2-6847.6)
	2 psi	9188.5 (7877.4-11267.0)	9405.8 (8508.8-10610.6)	8210.9 (7471.6-9144.5)

Peak principal logarithmic strain (LEP) did not demonstrate any trends with respect to the loading conditions, and was therefore the sole marker that was invariant across the applied loading conditions. The average threshold value for LEP for the nine cases reported was 0.188 +/- 0.032.

DISCUSSION

In this investigation, we estimated the threshold for mechanical injury to the blood-brain barrier by conducting a finite element analysis of Dynamic Cortical Deformation, an animal model of blood-brain barrier damage. We validated the finite element model with experimental data of the displacement of the cortex inferior to the craniectomy. By comparing elemental variables to experimental tissue on a one-to-one basis, we predicted threshold values for maximum principal logarithmic strain (LEP), maximum principal stress (SP), strain energy density (SEN), and von Mises stress (MIS). Furthermore, by exercising the finite element model at the multiple loading conditions used experimentally, we determined that LEP was the best predictor for damage, since this remained statistically invariant across loading conditions.

There are several key computational model features that should be considered when interpreting these results. Although the overall anatomic shape of the rat brain and skull were preserved in this model, we did not model the gray/white matter anatomy or the internal ventricular system. In addition, we assumed an interfacial condition between the brain and the skull because of the lack of quantitative experimental data on this condition. Finally, we proposed that the rat brain behaved similarly to human brain tissue, and therefore could be modeled using a constitutive law developed for the human brain.

These modeling assumptions more likely affect the value of the threshold prediction rather than the confidence in a particular threshold, or trends among various predictions. First, the inclusion of gray/white matter and the ventricular spaces in the finite element model alters the strain pattern and, in turn, threshold values by introducing local stress concentrations. Second, the boundary condition between the skull and brain will directly influence the extent of tissue deformed by the applied pressure pulse. However, even with considerable sliding in the current simulations, the brain tissue is deformed very focally. Increasing the frictional interaction will lower the amount of brain displacement through the craniectomy and increase frictional stresses along the periphery of the craniectomy. Finally, different material constants will affect the magnitude of stress and strain, but these effects will appear consistently across

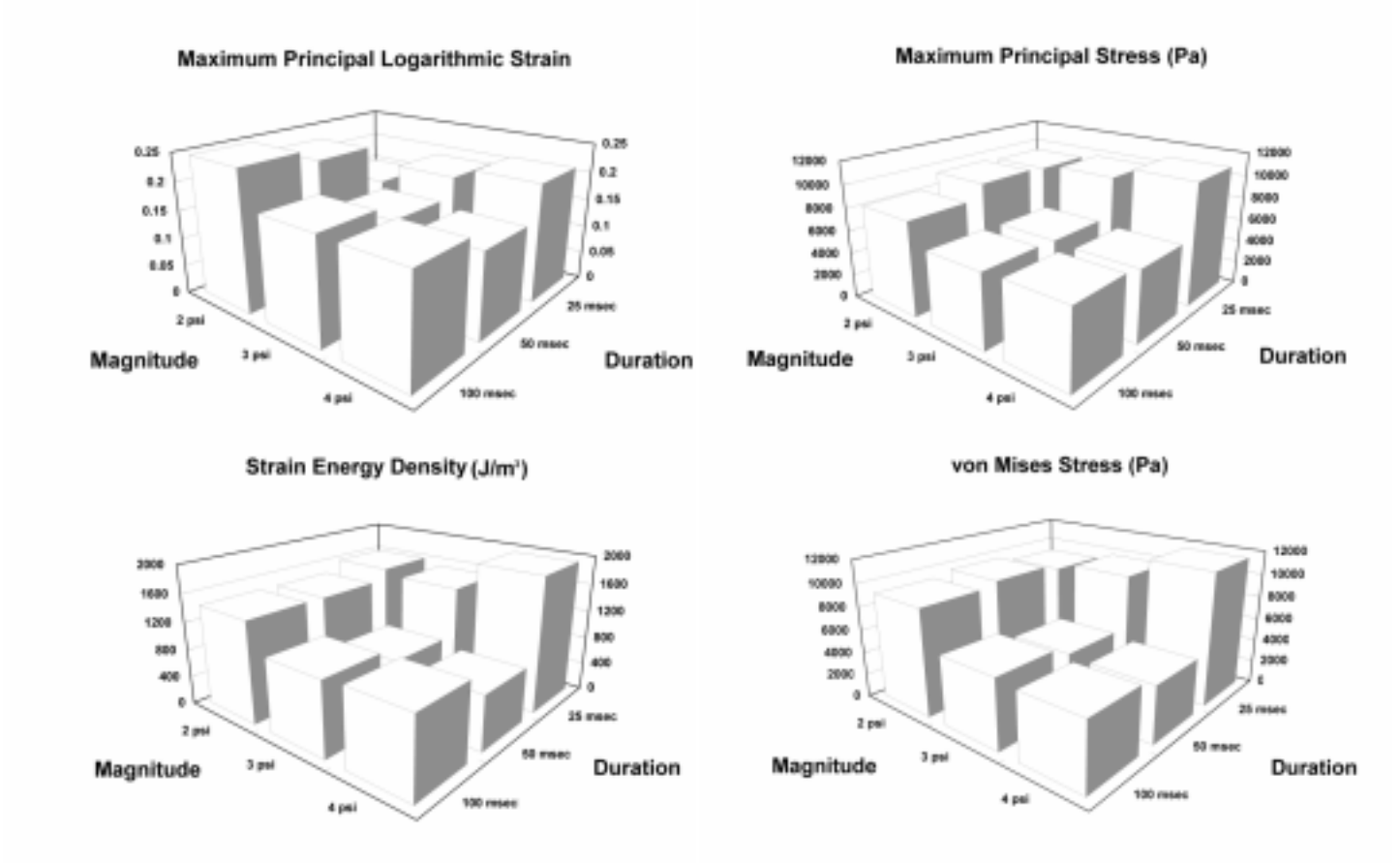

Figure 13: Three dimensional plots of 50th percentile threshold values for the four variables. Only LEP did not demonstrate a consistent trend with respect to the experimental loading conditions.

loading levels if the transient material behavior remains the same. None of these, however, are likely to dramatically change the general appearance of the deformation profile. Furthermore, all of these conditions would be present for every loading condition. Thus, changes due to these assumptions should consistently appear across all loading conditions and would, therefore, be unlikely to affect the results other than the magnitude of the threshold prediction.

One assumption which may affect the conclusions of this investigation is the selection of a hyperelastic-viscoelastic material law for brain tissue. Experimental studies of the material properties of brain tissue have demonstrated the non-linear behavior of the tissue at finite strains [27, 28]. Numerous studies have also shown the viscoelastic nature of brain tissue [27-31, 36, 37]. Most finite element simulations of TBI assume a linear elastic or linear elastic/viscoelastic material law [3, 5, 7-9, 38]. In a simulation of DAI, Mendis described a non-linear viscoelastic material law that was based on data from finite strain experiments on human brain tissue [25, 28]. A hyperelastic material law is attractive because it is based on a strain energy density function, which is easily incorporated into finite element codes, and because it is valid for the finite deformations we anticipated. Unfortunately, no data concerning the material response of rat brain tissue exists. However, with the hyperelastic-viscoelastic material law and stated constants, the computational model compared very well to experimental measurements of the displacement of the cortex. To ensure that our results are not excessively sensitive to changes in our assumptions, we are currently performing a parametric study on the material and geometric properties of the computational model.

Of course, the threshold values predicted in this investigation are for the BBB of the rat, and not for the human. Therefore, they should be viewed as estimates of human thresholds. However, whereas global, "whole-brain" organization may vary tremendously from species to species (e.g., number of gyri, presence of a falx, gray/white matter ratio, orientation of neuraxis, etc.), evidence suggests that, at the tissue and cellular level, inter-species brains respond similarly [27, 28]. For this reason, we believe that rat cortex and human cortex are similar enough that (1) the values predicted for threshold damage in the rat can serve as benchmarks for injury in the human, and (2) the determination of LEP as the best predictor of mechanically mediated injury to the BBB is valid for humans. Thus, although results from simulations of animal models may not directly reflect the response of the human brain, at worst they provide

benchmark tolerances to apply to the human models described above.

This represents the first attempt at quantifying in vivo mechanical thresholds for a specific form of cerebrovascular injury - BBB breakdown - in an animal model of TBI. Gennarelli et al. provided an analysis of the whole brain motions that could occur in a rapid noncentroidal rotation of the nonhuman primate head to produce cerebral contusions, but did not extend this analysis into predicting the intracranial movements and deformations during this inertial loading [39]. Lee et al. predicted the motions and strains occurring along the brain surface in sagittal plane head motions, but focused on the tearing of parasagittal bridging veins along the cortical surface [40]. Most recently, Ueno et al. reported correlations of shear strain and von Mises stress to cerebrovascular hemorrhage, but did not propose specific values nor examine the extent of BBB damage [8].

At first, this mechanical threshold for BBB damage may seem relatively low in comparison to a failure threshold (51% ultimate strain) for another cerebrovascular element, the parasagittal bridging veins [40]. However, the threshold developed in our analysis is not a predictor of complete structural failure and vascular hemorrhage. Strictly interpreted, a threshold LEP value of 0.188 implies that the BBB can withstand 19% natural strain before damage sufficient to allow particles 60 kD (the size of serum albumin) or smaller to pass into the parenchyma occurs. This methodology can be repeated with particles of different sizes using immunocytochemical techniques, as well as markers for red blood cells, to arrive at strain thresholds that predict a spectrum of BBB damage up to overt hemorrhage.

One of the most important findings from this study is that mechanical strain is a better measure for damage to the BBB than stress. This finding is due principally to the viscoelastic behavior of the brain tissue and, in turn, the brain response to the applied loading conditions. Most recent studies of the material properties of brain tissue, including the study we used to represent the brain in our finite element analysis, use two time constants to define a viscoelastic law for brain tissue. The first, and more dominant, time constant ranges from 5 to 25 msec [25, 27, 28, 30, 36]. This time constant dramatically increases the effective stiffness of brain tissue for extremely rapid loading, such as the 25 msec duration cases. For slower rates, the effective stiffness decreases, and the brain tissue deforms more readily.

The 50 msec and 100 msec duration experiments, in comparison to the 25 msec experiments, demonstrate the influence of the effective brain stiffness on the resulting injury pattern. The loading rates for the 50 and 100 msec experiment sets fall between the first and second time constants used to describe the brain viscoelastic behavior. Thus, the effective stiffness of the brain at these two longer rates is essentially equal. Subsequently, the strain fields for these loading rates are similar, and the volumes of injury are statistically indistinguishable for equal magnitudes of vacuum pressure. However, the strain for these rates would be greater and the stress would be less than for the remaining experimental set, the 25 msec duration cases. Post-hoc statistical examination of the experimental data revealed that the extent of BBB damage increased significantly with an increase in duration from 25 msec to 50 msec. Thus, because the volume of injury increased from the high onset rate (25 msec) to the slow onset rate (50, 100 msec), experimental injury to the BBB is more sensitive to strain than stress.

The results presented herein cannot be viewed as an absolute statement with regards to mechanical thresholds for the BBB, but rather as a first step towards definitively identifying a measure to predict BBB breakdown. In addition to improvements to the computational model, the general methods should be repeated with another model of TBI that induces BBB breakdown, such as fluid percussion or cortical impact, to ensure that the trends and thresholds identified for DCD hold for other types of loading conditions. Furthermore, we only investigated four mechanical parameters that have been cited as possible mediators of injury. This is not say that some other measure may not outperform these four. However, of the four studied, LEP was the most invariant predictor of BBB damage.

In a larger context, the analysis presented in this report can easily extend into other rodent models of TBI to study the injury thresholds for different tissues, as well as the invariance of these thresholds across all models. Rodents are by far the most frequently used animal in experimental TBI. Researchers in the neuroscience community use models such as fluid percussion, cortical impact, weight drop, and modified weight drop with the rat to discern mechanisms of cell death, understand functional and behavioral deficits, and identify potential pharmacological means of intervention following TBI. The ability to understand the underlying biomechanics of these injury models, and to compare the results to different measures of neurophysiological, functional, and behavioral injury, could prove to be an invaluable tool for injury research and prevention.

CONCLUSION

The protocol introduced in this investigation to investigate the biomechanics of TBI, identify threshold values for different measures of mechanically mediated BBB injury, and distinguish the utility of these measures, could prove to be useful for other forms of TBI as well. In this study, LEP proved to be the most invariant predictor of BBB breakdown. However, a different value and/or measure may prove to be more consistent for other primary pathologies, such as DAI. By recognizing

the individual nature of thresholds for various form of TBI, we can begin to develop more stringent and specific means and measures of injury prevention.

ACKNOWLEDGMENTS

Funding for this study was provided by the NIH 1RO1 NS35712-01, CDC R49/CCR 312712-01, and the Ashton Foundation.

REFERENCES

1. Sauren, AA and MHA Claessens. *Finite element modeling of head impact: The second decade*. in *International Conference on the Biokinetics of Impact (IRCOBI)*. 1993. Eindhoven, The Netherlands.

2. Khalil, TB and DC Viano. *Critical issues in finite element modeling of head impact*. in *26th Stapp Car Crash Conference*. 1982: SAE.

3. Ward, C, M Chan, and A Nahum. *Intracranial pressure - a brain injury criterion*. in *Stapp Car Crash Conference*. 1980: SAE.

4. Ruan, JS, T Khalil, and AI King, *Dynamic response of the human head to impact by three-dimensional finite element analysis.* Journal of Biomechanical Engineering, 1994. **116**: p. 44-50.

5. Chu, CS, MS Lin, HM Huang, and MC Lee, *Finite element analysis of cerebral contusion.* Journal of Biomechanics, 1993. **27**(2): p. 187-194.

6. Nahum, AM, R Smith, F Raasch, and C Ward. *Intracranial pressure relationships in the protected and unprotected head*. in *23rd Stapp Car Crash Conference*. 1979: Society of Automotive Engineers.

7. Bandak, FA and RH Eppinger. *A three-dimensional finite element analysis of the human brain under combined rotational and translational accelerations*. in *38th Stapp Car Crash Conference*. 1994: SAE.

8. Ueno, K, JW Melvin, L Li, and JW Lighthall, *Development of tissue level brain injury criteria by finite element analysis.* Journal of Neurotrauma, 1995. **12**(4): p. 695-706.

9. Zhou, C, TB Khalil, and AI King. *A new model comparing impact responses of the homogeneous and inhomogeneous human brain*. in *39th Stapp Car Crash Conference*. 1995. San Diego, CA: SAE.

10. Lighthall, JW, *Controlled cortical impact: A new experimental brain injury model.* Journal of Neurotrauma, 1988. **5**: p. 1-15.

11. Bandak, FA, RH Eppinger, and F DiMasi. *Assessment of traumatic brain injury using automotive crash tests and finite element analysis*. in *AGARD Head Injury Specialist Meeting*. 1996. Mescalero, NM.

12. Miller, RT, DH Smith, B Xu, TK McIntosh, and DF Meaney. *The role of kinetic loading parameters on the severity of diffuse axonal injury in close head injury*. in *AGARD Head Injury Specialist Meeting*. 1996. Mescalero, NM.

13. Mendis, KK, *Finite Element Modeling of the Brain to Establish Diffuse Axonal Injury Criteria*, in *Mechanical Engineering*. 1992, The Ohio State University: Columbus, OH.

14. Adams, JH, DI Graham, G Scott, LS Parker, and D Doyle, *Brain damage in fatal non-missile head injury.* Journal of Clinical Pathology, 1980. **33**: p. 1132-1145.

15. Cervós-Navarro, J and JV Lafuente, *Traumatic brain injuries: structural changes.* Journal of the Neurological Sciences, 1991. **102**: p. S3-S14.

16. Moos, T and K Molgard, *Cerebrovascular permeability to azo dyes and plasma proteins in rodents of different ages.* Neuropathology and Applied Neurobiology, 1993. **19**: p. 120-127.

17. Betz, AL, F Iannotti, and JT Hoff, *Brain edema: a classification based on blood-brain barrier integrity.* Cerebrovascular and Brain Metabolism Reviews, 1989. **1**: p. 133-154.

18. Dhillon, HS, D Donaldson, RJ Dempsey, and MR Prasad, *Regional levels of free fatty acids and Evans Blue extravasation after experimental brain injury.* Journal of Neurotrauma, 1994. **11**(4): p. 405-415.

19. Dietrich, WD, R Busto, M Halley, and I Valdes, *The importance of brain temperature in alterations of the blood-brain barrier following cerebral ischemia.* Journal of Neuropathology and Experimental Neurology, 1990. **49**(3): p. 486-497.

20. Smith, SL, PK Andrus, Z J.R., and ED Hall, *Direct measurement of hydroxyl radicals, lipid peroxidation, and blood-brain barrier disruption following unilateral cortical impact head injury in the rat.* Journal of Neurotrauma, 1994. **11**(4): p. 393-404.

21. Nawashiro, H, K Shima, and H Chigasaki, *Blood-brain barrier, cerebral blood flow, and cerebral plasma volume immediately after head injury in the rat.* Acta Neurochirurgica (Suppl), 1994. **60**: p. 440-442.

22. Povlishock, JT, DP Becker, HA Kontos, and LW Jenkins, *Neural and vascular alterations in brain injury*, in *Neural Trauma*, AJ Popp, Editor. 1979, Raven Press: New York. p. 79-93.

23. Povlishock, JT and HA Kontos, *The role of oxygen radicals in the pathobiology of traumatic brain injury.* Human Cell, 1992. **5**(4): p. 345-353.

24. Paxinos, G and C Watson, *The Rat Brain in Stereotaxic Coordinates*. 2nd ed. 1986, San Diego: Academic Press, Inc.

25. Mendis, KK, RL Stalnaker, and SH Advani, *A constitutive relationship for large deformation finite element modeling of brain tissue.* Journal of Biomechanical Engineering, 1995. **117**: p. 279-285.

26. Arbogast, KB, DF Meaney, and LE Thibault. *Biomechanical characterization of the constitutive relationship for the brainstem*. in *39th Stapp Car Crash Conference*. 1995. San Diego, CA.

27. Arbogast, KB, *A characterization of the anisotropic mechanical properties of the brainstem*, in *Bioengineering*. 1997, University of Pennsylvania: Philadelphia.

28. Galford, JE and JH McElhaney, *A viscoelastic study of scalp, brain, and dura.* Journal of Biomechanics, 1970. **3**: p. 211-221.

29. Fallenstein, GT, VD Hulce, and JW Melvin, *Dynamic mechanical properties of human brain tissue.* Journal of Biomechanics, 1969. **2**: p. 217-226.

30. Shuck, LZ and SH Advani, *Rheological response of human brain tissue in shear.* Journal of Basic Engineering, 1972: p. 905-911.

31. McElhaney, JH, RL Stalnaker, and MS Estes. *Dynamic mechanical properties of scalp and brain*. in *6th Annual Rocky Mountain Bioengineering Symposium*. 1969.

32. Hosmer, DW and S Lemeshow, *Applied Logistic Regression*. 1989, New York: John Wiley & Sons, Inc.

33. Kroell, CK, SD Allen, CY Warner, and TR Perl. *Interrelationship of velocity and chest compression in blunt thoracic impact to swine II*. in *30th Stapp Car Crash Conference*. 1986. San Diego, CA: SAE.

34. McIntosh, AS, D Kallieris, R Mattern, and E Miltner. *Head and neck injury resulting from low velocity direct impact*. in *37th Stapp Car Crash Conference*. 1993. San Antonio, TX: SAE.

35. Ridella, SA and DC Viano. *Determining tolerance to compression and viscous injury in frontal and lateral impacts*. in *34th Stapp Car Crash Conference*. 1990. Orlando, FL: SAE.

36. Bain, AC, KL Billiar, DI Shreiber, TK McIntosh, and DF Meaney. *In vivo mechanical thresholds for traumatic axonal damage*. in *AGARD Specialists Meeting*. 1996. Mescalero, N.M.

37. Metz, H, J McElhaney, and AK Ommaya, *A comparison of the elasticity of live, dead, and fixed brain tissue.* Journal of Biomechanics, 1970. **3**: p. 453-458.

38. Ruan, JS, TB Khalil, and AI King, *Human head dynamic response to side impact by finite element modeling.* Journal of Biomechanical Engineering, 1991. **113:** p. 276-283.

39. Gennarelli, TA, JM Abel, H Adams, and DI Graham. *Differential tolerance of frontal and temporal lobes to contusion induced by angular acceleration*. in *23rd Stapp Car Crash Conference*. 1979: Society of Automotive Engineers.

40. Lee, M and R Haut, *Insensitivity of tensile failure properties of human bridging veins to strain rate: implications in biomechanics of acute subdural hematoma.* Journal of Biomechanics, 1989. **22**: p. 537-542.

APPENDIX A

Constants and chi-squared values for the complete set of logistic regressions (P<0.00001 for all chi-squared tests). The constants α and β are determined after the logit transformation ($g(x)$):

$$\pi(x) = \frac{e^{\alpha+\beta x}}{1+e^{\alpha+\beta x}} \qquad g(x) = ln\left[\frac{\pi(x)}{1-\pi(x)}\right] = \alpha + \beta x$$

Loading Condition	Measure	α	β	χ^2
4 psi, 25 msec	LEP	-2.175	10.454	167.7
	SP	-1.470	1.29E-04	117.4
	SEN	-1.267	6.59E-04	99.9
	MIS	-2.169	2.02E-04	158.1
3 psi, 25 msec	LEP	-2.402	12.822	172.1
	SP	-2.137	2.21E-04	184.3
	SEN	-1.767	1.18E-03	141.4
	MIS	-2.583	2.67E-4	180.1
2 psi, 25 msec	LEP	-2.019	12.423	69.7
	SP	-1.677	1.87E-04	51
	SEN	-1.272	8.05E-04	20.3
	MIS	-1.949	2.12E-04	53.1
4 psi, 50 msec	LEP	-3.224	21.772	679.2
	SP	-2.503	5.20E-4	624.1
	SEN	-2.216	2.89E-03	645.3
	MIS	-3.567	5.85E-04	707.7
3 psi, 50 msec	LEP	-3.086	20.148	443.5
	SP	-2.471	4.91E-04	420.4
	SEN	-2.152	2.60E-03	422.8
	MIS	-3.504	5.62E-04	469.5
2 psi, 50 msec	LEP	-2.830	12.693	103.8
	SP	-3.529	3.70E-4	233.3
	SEN	-2.285	1.60E-3	96.9
	MIS	-3.022	3.21E-4	117.6
4 psi, 100 msec	LEP	-2.372	13.151	444.7
	SP	-1.850	3.30E-4	429.9
	SEN	-1.708	1.58E-3	439
	MIS	-2.554	3.45E-04	474.3
3 psi, 100 msec	LEP	-2.659	14.593	442.3
	SP	-2.200	3.73E-04	442.4
	SEN	-1.957	1.89E-3	419.9
	MIS	-2.816	4.45E-4	464.2
2 psi, 100 msec	LEP	-2.682	10.9	130.6
	SP	-2.933	3.21E-04	222.4
	SEN	-2.296	1.60E-03	143.1
	MIS	-2.905	3.54E-4	152.8